A Midlatitude–ENSO Teleconnection Mechanism via Baroclinically Unstable Long Rossby Waves

ELI GALANTI AND ELI TZIPERMAN

Environmental Sciences, Weizmann Institute, Rehovot, Israel

(Manuscript received 11 September 2002, in final form 24 January 2003)

ABSTRACT

The possibility of generating decadal ENSO variability via an ocean teleconnection to the midlatitude Pacific is studied. This is done by analyzing the sensitivity of the equatorial stratification to midlatitude processes using an ocean general circulation model, the adjoint method, and a quasigeostrophic normal-mode stability analysis. It is found that, on timescales of 2–15 yr, the equatorial Pacific is most sensitive to midlatitude planetary Rossby waves traveling from the midlatitudes toward the western boundary and then to the equator. Those waves that propagate through baroclinically unstable parts of the subtropical gyre are amplified by the baroclinic instability and therefore dominate the midlatitude signal arriving at the equator. This result implies that decadal variability in the midlatitude Pacific would be efficiently transmitted to the equatorial Pacific from specific areas of the midlatitude Pacific that are baroclinically unstable, such as the near-equatorial edges of the subtropical gyres (15°N and 12°S). The Rossby waves that propagate via the baroclinically unstable areas are of the advective mode type, which follow the gyre circulation to some degree and arrive from as far as 25°N and 30°S in the east Pacific. It is shown that the baroclinic instability amplifying these waves involves critical layers due to the vertical shear of the subtropical gyre circulation, at depths of 150–200 m.

1. Introduction

ENSO's decadal variability (e.g., An and Wang 2000; Trenberth and Hurrell 1994) has been the subject of quite a few studies during the past decade or so. Because typical timescales at the equator are relatively short, a strong candidate for this equatorial decadal variability is the slower midlatitude ocean, which somehow affects the equatorial ocean (e.g., Gu and Philander 1997; Jin et al. 2001; Kleeman et al. 1999). Gu and Philander (1997) suggested that the decadal variability in the Equatorial Pacific is a result of surface midlatitude water sinking along isopycnals toward the central Pacific equatorial thermocline base, where it upwells to the surface to affect the SST. The warmer SST, in turn, aside from changing the characteristics of ENSO (strength, period, etc.) also affects the midlatitude westerlies through the Tropic–extratropic temperature gradient. The stronger westerlies in the midlatitudes enhance evaporative cooling and create colder water that sinks and is advected toward the equator by the ocean general circulation, to later cool the SST there. The result is an interdecadal oscillation with an amplitude of about 1°C SST anomaly.

Corresponding author address: Eli Galanti, International Research Institute for Climate Prediction, The Earth Institute at Columbia University, Rm. 202, Monell Bldg., Lamont-Doherty Earth Observatory, 61 Route 9W, Palisades, NY 10964-8000.
E-mail: eli@iri.columbia.edu

This scenario was modified in various ways by other studies. Some focused on pure oceanic pathways between the midlatitude and the equatorial region either through along-isopycnal advection (Harper 2000; Zhang et al. 2001) or through planetary waves propagating from midlatitudes to the Tropics (Jin et al. 2001; Liu 1999a; Lysne et al. 1997). Other studies have emphasized the role of planetary waves within the Tropics (Capotondi and Alexander 2001; Jin 2001). Repeat hydrography observations show eddy motions that may perhaps be interpreted as planetary waves (e.g., Roemmich and Gilson 2001). Some other studies seemed to find that oceanic teleconnections are not efficient (Hazeleger et al. 2001) and others that the oceanic teleconnection is mostly active in the Southern Hemisphere (Schneider et al. 1999). An alternative atmospheric bridge via which atmospheric influence propagates to the Tropics has also been suggested (Barnett et al. 1999). Another study (Kleeman et al. 1999) emphasized the role of midlatitude anomalous winds (which may be a response to equatorial SST anomalies) in producing SST anomalies along the equator by changing the strength of the subtropical cells, and as a consequence the rate of upwelling along the equator. A related work dealing with changes to the subtropical meridional cells is of McPhaden and Zhang (2002).

The question of what is the relative importance of the two oceanic teleconnection mechanisms (subduction vs waves) in transferring decadal signals from the midlat-

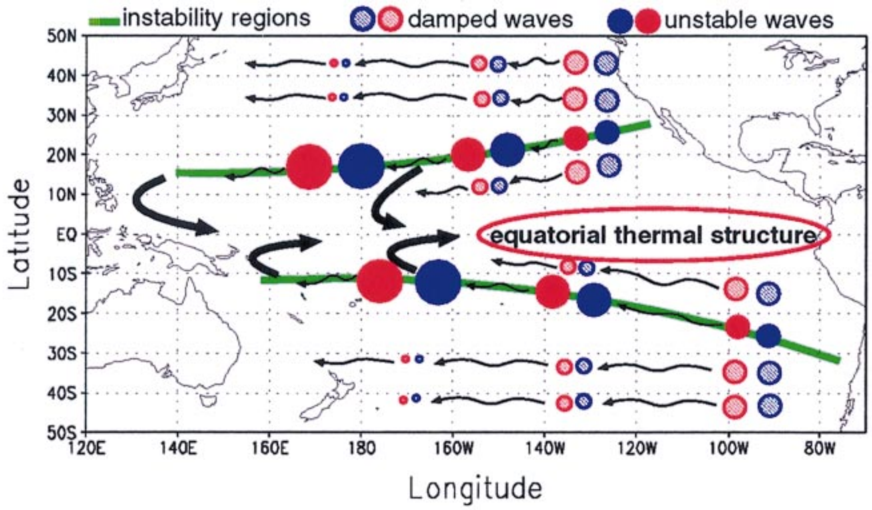

FIG. 1. A schematic figure of the mechanism proposed in this paper for a wave teleconnection from the midlatitude Pacific to the equator. Midlatitude planetary Rossby waves travel westward at all latitudes and are damped. The waves that are amplified in baroclinically unstable regions of the subtropical gyre arrive to the equator with a larger amplitude and therefore dominate the midlatitude signal there.

itudes to the equator is still unanswered. Another unresolved issue in these works is what selects the particular midlatitude areas from which Rossby waves arrive to influence the equatorial Pacific.

In this work we attempt a new approach to the study of possible oceanic teleconnections from the midlatitudes to the equatorial Pacific. We use the adjoint method of sensitivity studies (Galanti et al. 2002; Hall and Cacuci 1983; Marotzke et al. 1999) with an ocean general circulation model (GCM) to determine what are the midlatitude locations and physical processes that influence the equatorial region within a decadal timescale. We find that long Rossby waves that propagate from as far as 25°N and 30°S are the dominant mechanism that transmits information from the midlatitudes to the equator in our model. Furthermore, we find that the waves that are especially effective in transmitting information from the midlatitudes to the equator travel mostly along specific latitude bands (15°N and 12°S). By analyzing the quasigeostrophic normal modes for the model background state, we show that the model climatology is baroclinically unstable at the latitudes where the sensitivities are seen. The Rossby waves that are able to affect substantially the equatorial thermal structure seem to be of the ''advective mode'' type (Liu 1999b), which tend to follow the gyre circulation fairly closely yet are distinct from an advection by the gyre circulation.

Figure 1 therefore summarizes our main finding here. Rossby waves travel from all latitudes of the Pacific Ocean toward the western boundary and then travel as coastal Kelvin waves to affect the equator. However, only the waves that travel along baroclinically unstable parts of the midlatitude gyre (mostly the southern edge of the gyre in the North Pacific and northern edge in the South Pacific) are amplified by baroclinic instability. Waves at other latitudes are damped by various dissipative mechanisms and do not make it to the equator. The Rossby waves that travel along the baroclinically unstable areas reach the equator with a larger amplitude and dominate the midlatitude signal that affects the basic stratification there.

The paper is organized as follows. In section 2 we describe the ocean model and the adjoint method used in the study. The adjoint sensitivity results are presented in section 3 together with an analysis of the sensitivity dynamics. Section 4 analyzes the normal-mode quasigeostrophic (QG) stability of the model background climatology, and the results are compared with the sensitivity structure from the adjoint model runs. We conclude in section 5.

2. The model

The ocean model we use and its adjoint were described in details by Galanti et al. (2002). It was used for sensitivity studies of the equatorial Pacific ocean–atmosphere instability mechanism (Galanti et al. 2002), as well as for investigating ENSO predictability based on the adjoint method of data assimilation (Galanti et al. 2003). Here we give a brief description of the model components.

The ocean model is based on the Geophysical Fluid Dynamics Laboratory (GFDL) Modular Ocean Model (an early alpha version of MOM4) (Pacanowski and Griffies 1999). The model domain is the Indo–Pacific region, 50°S–50°N, 130°E–70°W. The model resolution is 3° in longitude, 3° going to 1° at the equator in latitude, and 30 depth levels, where the top 15 layers are within the top 200 m of the ocean. The resolution is such that the equatorial dynamics (Kelvin and Rossby waves) are resolved, while the computational cost is small enough to enable many long model runs.

The model uses a modified Richardson-number-dependent vertical mixing scheme (Pacanowski and Philander 1981; Syu and Neelin 2000). In addition, a simplified mixed layer scheme is applied as in Syu and Neelin (2000). Constant horizontal viscosity and diffusivity are used. The temperature and salinity are restored to the monthly Levitus (1982) climatology within sponge layers at the north and south horizontal boundaries.

The model is spun up forced by the climatological FSU wind stress (Stricherz et al. 1997; Stricherz et al. 1992) and climatological heat fluxes (Esbensen and Kushnir 1981). The model is also restored to the climatological monthly National Centers for Environmental Prediction (NCEP) SST (Reynolds and Smith 1994) and to the climatological monthly Levitus sea surface salinity (SSS) (Levitus 1982) with a restoring time of 10 days. After reaching its mean seasonal climate state (50 years of spinup), the monthly mean model air–sea flux is saved to be used as a fixed (changing monthly, but not year to year) heat flux forcing field. A weak restoring to the surface model climatology of 100 days is also applied during the model run. The monthly temperature climatology of the model under this monthly heat flux and weak restoring is similar to the Levitus climatology. Note that the fixed heat flux plus weak restoring allow the development of SST anomalies, whose suppression by a stronger restoring might have adversely affected our objectives here.

An adjoint model for the ocean model was derived with the help of the Tangent Linear and Adjoint Model Compiler (Giering 1999; Giering and Kaminski 1998; Marotzke et al. 1999). As the timescale of interest in this work is much longer than the timescale studied in Galanti et al. (2002), some modifications had to be made to the model and to its adjoint. The model vertical resolution is very coarse in the deep ocean, reaching grid size of about 600 m in the deepest level. The model thus exhibits a weak numerical instability that arises from the inaccuracy of the finite differencing scheme at the lower levels. In the forward run, this weak numerical instability is damped by the model nonlinearities and is observed as a small amplitude noise near the bottom. During the adjoint run, these instabilities grow, since the adjoint model is linear, so that at timescales of more than a few years the instabilities develop and influence the adjoint solution. In order to eliminate this problem we restored the adjoint solution of the temperature and salinity at the deepest model level to zero at each time step. We have run a few tests and found that this restoring does not introduce artifacts into our upper-ocean model results, which are of interest in this study.

The physical context of the adjoint sensitivity experiments is determined by the formulation of the cost function and by the choice of the control variables. The cost function is the scalar whose sensitivity is studied with respect to changes in the control variables; it can be any measure of the model state. The cost function we use is the same as the one used in Galanti et al. (2002). It is a summation over the subsurface model temperature in the equatorial east Pacific, where the temperature signal of the mature phase of ENSO is maximal:

$$J = \int d^3\mathbf{x}\, dt\, T(\mathbf{x}, t) \times \exp\left[-\frac{(x - 100°\mathrm{W})^2}{10°^2} - \frac{(y - 0°\mathrm{N})^2}{2°^2} - \frac{(z - 60\ \mathrm{m})^2}{(40\ \mathrm{m})^2} - \frac{t^2}{(10\ \mathrm{day})^2}\right], \qquad (1)$$

where $\mathbf{x} = (x, y, z)$. This cost function also reflects the status of the subsurface thermocline structure, whose changes may lead to decadal ENSO variability. The control variables we will look at are the temperature and salinity fields, as they determine the density field. Note that all adjoint sensitivities appearing in this work are normalized by the volume of the box they represent in such a way that the surface variables at the equator (smallest box volume) are normalized by a factor of 1 [see Galanti et al. (2002) and Marotzke et al. (1999) for an extensive discussion]. The normalization of the adjoint solution is done only when displaying and analyzing the results and not during the adjoint model integration.

3. Results

We now present the results from the adjoint model runs, along with results from two complementary experiments of the forward model that are helpful in the interpretation of the sensitivity results.

a. Decadal sensitivities

We ran the ocean model for 20 yr, during which it remained around its climatology, and then ran its adjoint over the same period backward in time. The adjoint model calculates the sensitivity of the cost function to perturbations in all model variables at all times between the time of the cost function evaluation and the time of the initial conditions. Figure 2 shows the sensitivity to temperature perturbations at a depth of 200 m 4, 8, and 12 years prior to the time of the cost function evaluation. A positive sensitivity somewhere in the middle panel means that a positive temperature perturbation applied at that location will lead to an increase of the cost func-

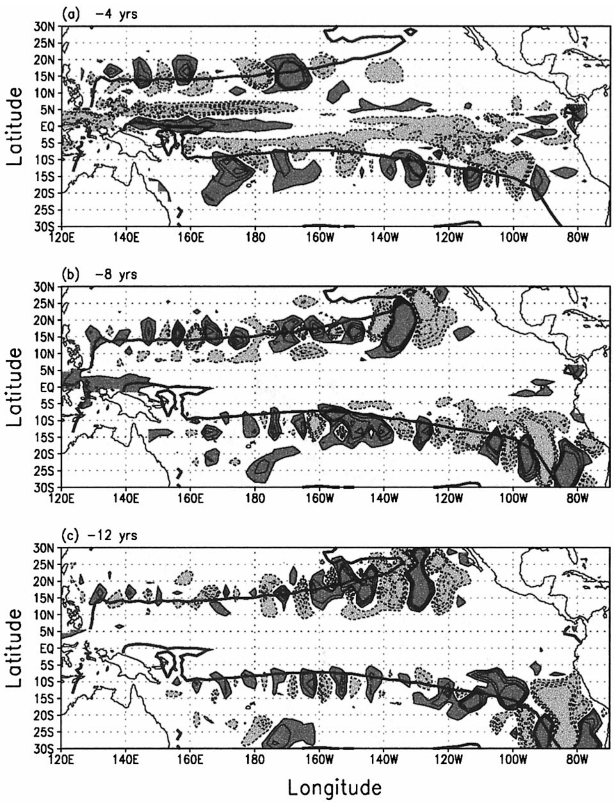

FIG. 2. Sensitivity to temperature perturbations at a depth of 200 m at time intervals of (a) 4, (b) 8, and (c) 12 yr before the time of cost function evaluation. Values larger (smaller) than 0.005 (−0.005) are shaded with dark (light) gray. The thick black line denotes the 16°C isotherm of the forward model climatology.

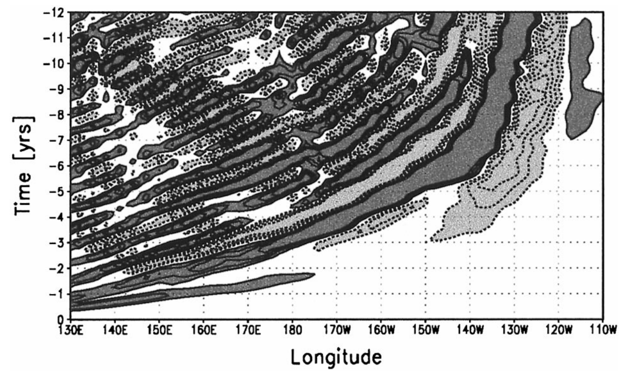

FIG. 3. Sensitivity to temperature perturbations at 15°N and depth of 200 m as function of longitude and time (in years before time of cost function evaluation). Values larger (smaller) than 0.005 (−0.005) are shaded with dark (light) gray.

tion (integrated temperature over the subsurface east equatorial Pacific) evaluated 8 years later. A negative sensitivity means that a positive perturbation will lead to a decrease of the cost function. The amplitude of the sensitivity indicates, for example, that a perturbation applied 4 years before the time of the cost function evaluation (Fig. 2a) at 15°N, 160°E is twice as effective in increasing the value of the cost function than a temperature perturbation at 13°N, 160°E at the same time. The main feature seen in the sensitivities is a wavelike pattern (which we will denote ''adjoint waves'' from now on) that is formed around latitudes 15°N and 12°S and travels eastward approximately along lines of constant temperature of the forward model climatology (thick black line in the figure). Upon reaching the east Pacific, the adjoint wave trajectory is bent toward 25°N and 30°S.

The eastward propagation of the adjoint sensitivity waves is further illustrated in Fig. 3, where the sensitivity to temperature perturbation at 15°N and a depth of 200 m is plotted as a function of longitude and time. The velocity of the adjoint waves west of 160°W is about 4 cm s^{-1} and east of 160°W is about 2 cm s^{-1}.

The sensitivities shown in Fig. 2 are the main result of this paper. As explained above, the adjoint model calculates the sensitivity of the cost function to perturbations to the model variables at different times and locations. Physically, the sensitivities in Fig. 2 indicates that temperature perturbations applied off the equator would influence the subsurface temperature in the east equatorial Pacific a few years later. This, of course, indicates some teleconnection mechanism between the equatorial and off equatorial areas of the Pacific ocean, which is what we are after in this study.

Another thing to remember is that the adjoint model is integrated backward in time. When interpreting a sensitivity pattern that propagates in time, the direction of propagation should therefore be reversed; the adjoint waves we see propagating *eastward* will be shown below to be an indication of a sensitivity to physical Rossby waves that propagate *westward.*

Figure 4 shows a cross section along 15°N at times of 4, 8, and 12 years before the time of cost function evaluation. The temperature sensitivities are located around a depth of 200 m and are also vertically tilted to the east. The 16°C isotherm of the forward model climatology is also plotted for reference. The main features seen in Fig. 4 are eastward-tilted wavelike sensitivities; these features indicate that applying perturbations in the forward model that have the same spatial eastward tilt will be most efficient in increasing the value of the cost function (that is, the subsurface equatorial temperature) a few years later. We will show in the following sections that these are sensitivities to midlatitude long Rossby waves and that baroclinic instability, hinted by this tilt, plays an important role in their development and amplification. A meridional cross section of the temperature anomalies shows that the sensitivities tend to be located in regions where the climatological meridional temperature gradient is largest (not shown), and we will discuss the relevance of this to baroclinic instability in the followings. The sensitivities in the Southern Hemisphere are somewhat less pro-

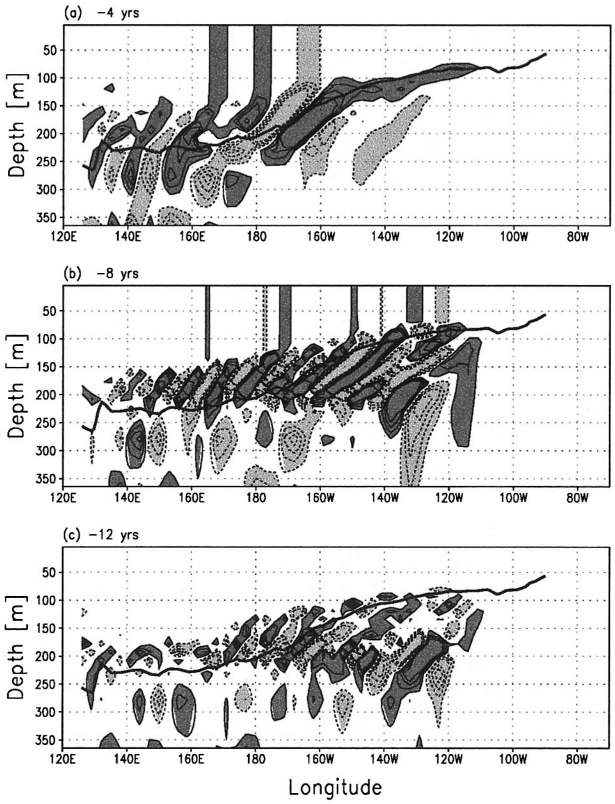

FIG. 4. Sensitivity to temperature perturbations at 15°N as function of longitude and depth, at time intervals of (a) 4, (b) 8, and (c) 12 yr before the time of cost function evaluation. Values larger (smaller) than 0.005 (−0.005) are shaded with dark (light) gray. The thick black line denotes the 16°C isotherm of the forward model climatology.

nounced and are stronger at the east Pacific, around 25°S.

We can conclude at this stage that at timescales from 2 to 15 yr the largest sensitivity of the east Pacific equatorial thermocline is to perturbations that travel westward (in the forward model) in the vicinity of 15°S and 12°N. In the next section we will show that these sensitivities indeed have the properties of midlatitude long Rossby waves; therefore the sensitivity signal seems to propagate from midlatitude not by advection (e.g., Gu and Philander 1997; Harper 2000) but rather through a dynamical process that involves planetary wave propagation.

b. Are these actually waves?

The first question we need to address is whether the above propagation signal of the sensitivities is really due to waves as it appears to be. Since the cost function is a summation over the east equatorial temperature, this question can be resolved by separating the sensitivities into a *dynamical* sensitivity and a *kinematic* sensitivity (Marotzke et al. 1999). A change in temperature can be due to a ''dynamical'' process such as internal wave propagation, which merely moves the isopycnal layers vertically. We clearly want to verify that our sensitivities correspond to such a dynamical sensitivity. Alternatively, the temperature can vary due to a ''kinematic'' process such as an advective or diffusive along-isopycnal intrusion process that modifies the temperature and salinity, leaving the density unchanged (Munk 1981). In both cases (of dynamical and kinematic sensitivities), the temperature and salinity sensitivities are not independent and can be shown to be related via the thermal and salinity expansion coefficients (Marotzke et al. 1999):

$$\alpha \equiv -\frac{1}{\rho}\left(\frac{\partial \rho}{\partial T}\right)_S; \qquad \beta \equiv \frac{1}{\rho}\left(\frac{\partial \rho}{\partial S}\right)_T. \tag{2}$$

Begin by writing the cost function J as a function of the density $[\rho(T, S)]$ and of the temperature (T) fields:

$$J = J[\rho(T, S), T]. \tag{3}$$

In writing the cost this way, we separate the influence on the cost function into the part that comes from vertically moving the isopycnal surfaces $[\rho(T, S)]$, and the part that comes from intrusion processes that modify the temperature, leaving the density unchanged. The sensitivity of the cost function J to the temperature T, at a constant salinity, is therefore

$$\begin{aligned}\left(\frac{\partial J}{\partial T}\right)_S &= \left(\frac{\partial J}{\partial \rho}\right)_T\left(\frac{\partial \rho}{\partial T}\right)_S + \left(\frac{\partial J}{\partial T}\right)_\rho \\ &= -\alpha\rho\left(\frac{\partial J}{\partial \rho}\right)_T + \left(\frac{\partial J}{\partial T}\right)_\rho,\end{aligned} \tag{4}$$

where the first and second terms on the rhs of (4) are the dynamical and kinematic sensitivities, respectively. The sensitivity of the cost function J to the salinity S is

$$\left(\frac{\partial J}{\partial S}\right)_T = \left(\frac{\partial J}{\partial \rho}\right)_T\left(\frac{\partial \rho}{\partial S}\right)_T = \beta\rho\left(\frac{\partial J}{\partial \rho}\right)_T. \tag{5}$$

The adjoint model actually calculates only $(\partial J/\partial T)_S$ and $(\partial J/\partial S)_T$. These may be used to calculate the two sensitivities by using (2), (4), and (5) so that

$$-\alpha\rho\left(\frac{\partial J}{\partial \rho}\right)_T = -\frac{\alpha}{\beta}\left(\frac{\partial J}{\partial S}\right)_T \text{ (dynamical)} \tag{6}$$

$$\left(\frac{\partial J}{\partial T}\right)_\rho = \left(\frac{\partial J}{\partial T}\right)_S + \frac{\alpha}{\beta}\left(\frac{\partial J}{\partial S}\right)_T \text{ (kinematic).} \tag{7}$$

Figure 5 shows the dynamic (6) and kinematic (7) sensitivities to temperature perturbations. It is clear that most of the sensitivity calculated by the adjoint model is dynamical. Kinematic sensitivity can be seen only around 15°S, 140°W and is much smaller than the dynamic sensitivity. We can therefore conclude that the adjoint sensitivities we observe in the model at time-

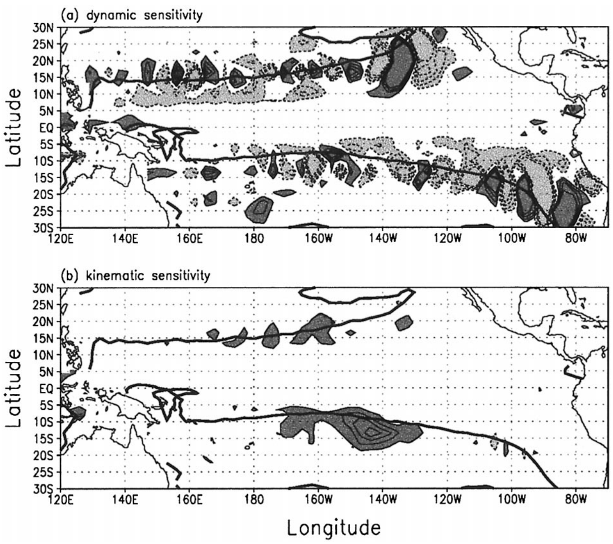

FIG. 5. Demonstrating that the adjoint signal is indeed due to waves: (a) dynamical sensitivity vs (b) kinematic sensitivity [see (6), (7)], 8 yr before the time of the cost function evaluation (contour lines and shading are as in Fig. 2). Dynamic sensitivity that corresponds to wave motions that vertically move the isopycnals is significantly larger than kinematic sensitivity which corresponds to long-isopycnal advection which does not change the density field.

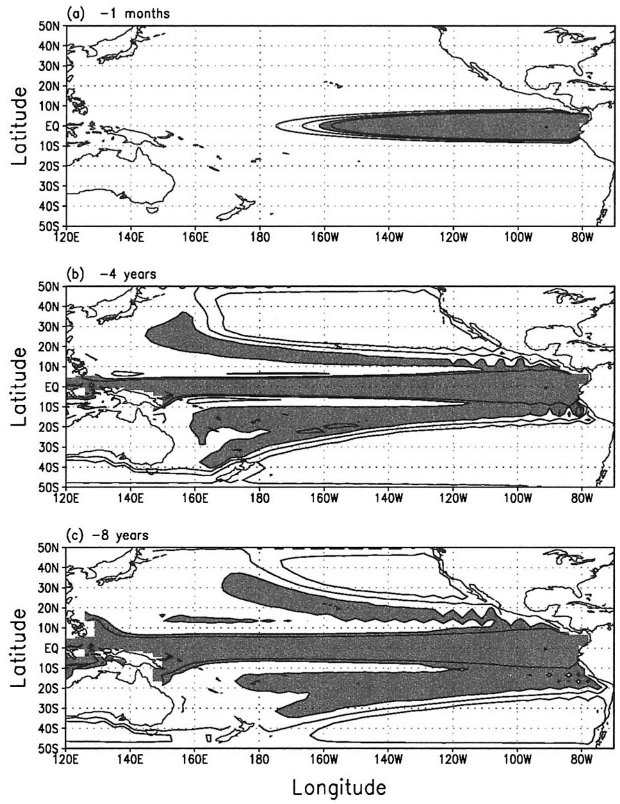

FIG. 6. Sensitivities to temperature perturbations at a depth of 200 m for the idealized model with horizontally uniform stratification: (a) 1 month, (b) 4 yr, and (c) 8 yr before the time of the cost function evaluation. Contour intervals in (a), (b), and (c) are 0.001, 0.000 75, and 0.0005, respectively. Values larger than 0.003, 0.002, and 0.0015 are shaded with dark gray in panels (a), (b), and (c), respectively.

scales of 2–15 yr are indeed dynamical sensitivities due to internal planetary wave motions, rather than along-isopycnal advection processes.

Another issue of importance is the relevance of the adjoint sensitivities to the actual ocean dynamics: the adjoint model indicates the perturbations to which the sensitivity is maximal, yet it does not provides any information on whether such perturbations are likely to occur. Given that we see sensitivities to upper ocean temperature perturbations in the midlatitude Pacific Ocean, we can be fairly confident that such perturbations will indeed occur due to natural decadal variability in that area. It is therefore likely that the sensitivity we see here will be excited by temperature anomalies that naturally occur and is therefore physically relevant.

c. What sets the path of propagation of the sensitivities?

An a priori consideration of the sensitivity problem would lead one to the expectation that Rossby waves from the entire midlatitude Pacific Ocean should propagate westward until they reach the western boundary. From that point the signal can propagate to the equator and there be transformed into an equatorial Kelvin wave, which affects the thermocline structure. Why then is it that only certain latitude bands around 15°N and 12°S affect the equator in our sensitivity runs? In order to address this question, we run an experiment in which the ocean model has the same geometry and bathymetry. The temperature initial conditions were set to a horizontally uniform idealized vertical profile that mimics a mixed layer (150 m deep), a main thermocline (at a depth of 200 m), and a weakly stratified deep ocean. The salinity was set to a uniform value of 35. No wind is applied. The adjoint of this model was then run with a similar cost function to that used above, centered at the depth of the idealized thermocline in the east Pacific.

Figure 6 shows that in this model the sensitivities indeed propagate from all latitudes as Rossby Waves and affect the eastern Pacific thermocline; this can be seen by comparing the snapshots in Figs. 6b and 6c of the figure and noting the eastward propagation of the adjoint signal that occurs between these snapshots at all midlatitude locations. The propagation is clearly faster toward the equator due to the faster Rossby wave propagation there. However, all sensitivities decay in the model within 2–3 yr (note the different contour levels used in the different panels), unlike the case in our model with observed climatological background (Fig. 2), where these sensitivities persist for 10–15 yr. Another difference is that sensitivities in our standard adjoint model run are restricted to two bands at 15°N and 12°S, while in the idealized model they are spread over all latitudes. A final difference between the standard and

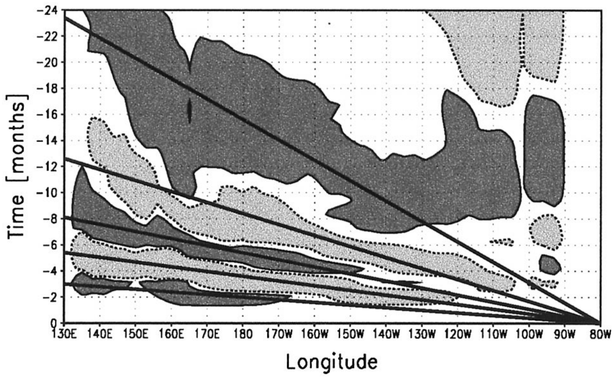

FIG. 7. Sensitivity to temperature perturbations along the equator at depth of 2200 m as function of months prior to time of cost function evaluation. Values larger (smaller) than 0.001 (−0.001) are shaded with dark (light) gray. The thick black lines indicate the approximate propagation of the sensitivities with time and longitude.

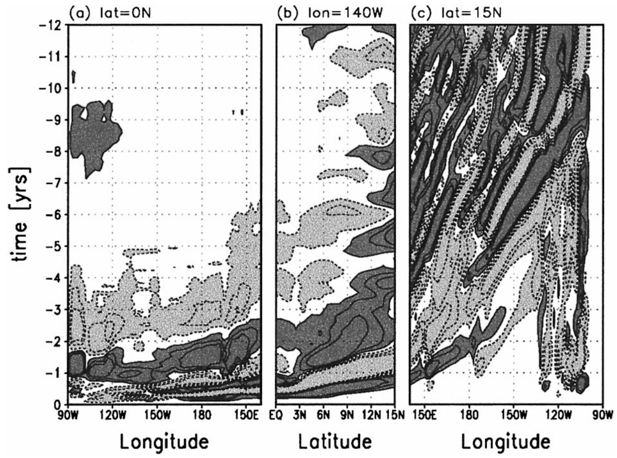

FIG. 8. The connection between the equator and 15°N: the time–space sensitivity to temperature perturbations at depth of 2200 m: (a) sensitivities along the equator (note that longitude axis is reversed), (b) sensitivities along 140°E between 0° and 15°N, (c) sensitivities along 15°N. Values larger (smaller) than 0.005 (−0.005) are shaded with dark (light) gray.

idealized runs is that the sensitivities in the standard run propagate eastward along 15°N and then turn northward up to 25°N, while in the idealized model the propagation is purely eastward.

Our conclusion from this section is that significant sensitivities exist mainly at 15°N (and 12°S) because of the structure of the background circulation and density field felt by the propagating waves and imposed by the midlatitude gyre circulation. The reason for the Rossby waves to favor these regions, and especially the season for their ability to persist over long periods of time, will be discussed below (section 4).

d. Sensitivities along the equator: The midlatitude–equator connection

So far we showed the sensitivity of the equatorial Pacific subsurface thermal structure to midlatitude perturbations at a time scale of a few years, but we are yet to show where and how these perturbations affect the equatorial region. Figure 7 shows the sensitivity of the subsurface east Pacific thermocline [i.e., the cost function equation in (1)] to temperature perturbations along the equator at a depth of 2200 m for the first 24 months prior to the cost function evaluation. The thick black lines indicate the approximate propagation of the sensitivities with time and longitude. The 2000-m depth is chosen because the wave signal is clearest there, although the wave modes seen are actually surface enhanced. It can be seen that the subsurface temperature (cost function) is sensitive to what seems to be different baroclinic Kelvin modes that travel all the way from the western Pacific (around 140°E). These modes propagate at different speeds and therefore affect the cost function region at different times. Note that the model's relative coarse meridional resolution might distort somewhat the shape and phase speed of the equatorial Kelvin waves; yet the results seen here should still be qualitatively valid.

We next try to identify the connection path between the sensitivities showing up along 15°N and those seen earlier at the equator. Figure 8a shows the sensitivities along the equator during a 12-yr adjoint model run; Fig. 8b shows the sensitivities at the region of the western boundary of the Pacific, 140°E, from the equator to 15°N; and Fig. 8c shows the sensitivities along 15°N, from 140°E to 80°W. The three panels illustrate the wave path from the 15°N region to the east equatorial region. Following the sensitivities backward, from Fig. 8c to Fig. 8a (forward in real time), we can see that a major part of the perturbations that start their way as long midlatitude Rossby waves travel westward to the western boundary (Fig. 8c), then travel as coastal Kelvin waves from 15°N to the equator (Fig. 8b), and eventually travel eastward as equatorial Kelvin waves to reach the eastern Pacific and affect the thermal structure there (Fig. 8a).

Some of the midlatitude Rossby wave sensitivities seen in Fig. 8c cannot be related to the above scenario. They seem to be transmitted from the equator to 15°N along 170°W as seen in Figs. 9a–c. The precise mechanism that allows this teleconnection is not clear and may have to do with a distortion of the background potential vorticity field that allows the midlatitude Rossby wave energy to leak from the midlatitudes toward the equator before reaching the western boundary.

4. An eigenmode stability analysis in the QG regime

The objective of this section is to demonstrate the role of baroclinic instability in amplifying the sensitivities and shaping their path, as hypothesized in the previous sections. We do this by assuming that the sensi-

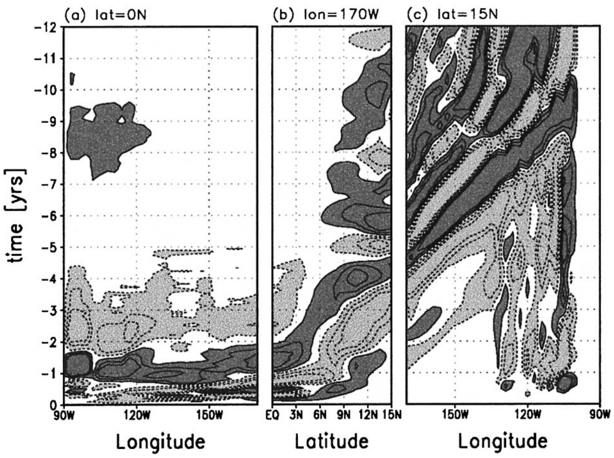

FIG. 9. As in Fig. 8 but for a connection along 170°W: (a) sensitivities along the equator (note that longitude axis is reversed), (b) sensitivities along 170°W between 0° and 15°N, (c) sensitivities along 15°N. Values larger (smaller) than 0.005 (−0.005) are shaded with dark (light) gray.

tivities are locally governed by QG dynamics, solving for the QG normal modes based on the forward model climatology and comparing the eigenmode solutions to the structure of the adjoint sensitivities.

Liu (1999b) showed that in the presence of a background shear flow, instead of the usual baroclinic modes, one finds a ''non-Doppler-shifted'' mode that resembles the first baroclinic mode and higher ''advective'' modes that tend to propagate following the path of the mean flow (see also Liu 1999a). The waves we see in the adjoint sensitivities seem to be of the advective kind, as they follow closely the mean gyre circulation. In addition to these complications due to the existence of a mean shear, we are also concerned with baroclinic instability and in particular with the existence of critical layers that seem to dominate the structure and growth of our adjoint sensitivity signal.

First, let us define the appropriate variables for the QG theory:

$$\rho = \rho_0 + \overline{\rho}(\mathbf{x}) + \rho'(\mathbf{x}, t) \tag{8}$$

$$(u, v) = [\overline{u}(\mathbf{x}), \overline{v}(\mathbf{x})] + [u'(\mathbf{x}, t), v'(\mathbf{x}, t)] \tag{9}$$

$$\psi = \overline{\psi}(\mathbf{x}) + \psi'(\mathbf{x}, t), \tag{10}$$

where $\mathbf{x} = (x, y, z)$; ρ, (u, v), and ψ are the density, horizontal velocity, and streamfunction fields. The averaged densities ρ_0 and $\overline{\rho}(x, y, z)$ were calculated from the model climatological temperature and salinity. The variables $\overline{u}$, $\overline{v}$ are the model climatological horizontal velocities. The buoyancy frequency $N(z)$ was calculated according to

$$N^2 = -\frac{g}{\rho_0}\frac{\partial\overline{\rho}}{\partial z}. \tag{11}$$

The buoyancy frequency N^2 is treated as if it were only a function of z when taking horizontal derivatives, following the QG approximation. We have set $N^2(z)$ to be no smaller than 10^{-7} s^{-2} (Killworth et al. 1997) and in the mixed layer region to be no smaller than 10^{-4} s^{-2}.

Noting that

$$u' = -\frac{\partial\psi'}{\partial y}, \quad v' = \frac{\partial\psi'}{\partial x}; \quad \rho' = -\frac{\rho_0 f_0}{g}\frac{\partial\psi'}{\partial z}, \tag{12}$$

the quasigeostrophic potential vorticity (PV) equation in the presence of background velocities (and horizontal density gradients) is

$$\left(\frac{\partial}{\partial t} + \overline{u}\frac{\partial}{\partial x} + \overline{v}\frac{\partial}{\partial y}\right)\left\{\frac{\partial^2\psi'}{\partial x^2} + \frac{\partial^2\psi'}{\partial x^2} + \frac{\partial}{\partial z}\left[\frac{f_0^2}{N(z)^2}\frac{\partial\psi'}{\partial z}\right]\right\} + \frac{\partial\psi'}{\partial x}\frac{\partial\overline{\Pi}}{\partial y} - \frac{\partial\psi'}{\partial y}\frac{\partial\overline{\Pi}}{\partial x} = \nu\nabla^4\psi', \tag{13}$$

where

$$\overline{\Pi} = f + \beta y + \left(\frac{\partial\overline{v}}{\partial x} - \frac{\partial\overline{u}}{\partial y}\right) - \frac{\partial}{\partial z}\left[\frac{f_0^2}{N(z)^2}\frac{g}{\rho_0 f_0}\overline{\rho}\right] \tag{14}$$

is the background potential vorticity. The term on the rhs of (13) represents the model eddy viscosity, where $\nu = 2 \times 10^4$ m^2 s^{-1} is the model horizontal viscosity coefficient. Assuming a solution of the form

$$\psi' = e^{i(kx+ly-\omega t)}h(z) \tag{15}$$

with the boundary conditions being

$$\frac{\partial\psi'}{\partial z} = 0 \quad \text{at } z = 0, z_B, \tag{16}$$

we can write (13) as

$$\begin{aligned}&\frac{\partial}{\partial z}\left[\frac{f_0^2}{N(z)^2}\frac{\partial h}{\partial z}\right] - (\overline{u}k + \overline{v}l - \omega)^{-1} \\ &\quad\times\left[(\overline{u}k + \overline{v}l - \omega)(k^2 + l^2) + k\frac{\partial\overline{\Pi}}{\partial y} - l\frac{\partial\overline{\Pi}}{\partial x}\right. \\ &\qquad\left. + \nu(k^2 + l^2)^2\right]h = 0,\end{aligned} \tag{17}$$

which is the familiar eigenproblem, ω being the eigenvalue and $h(z)$ being the eigenfunction. We chose to solve the eigenproblem by writing the derivative in z in centered finite difference form and rearranging the equation into a matrix form of a generalized eigenproblem,

$$\mathbf{A}h = \omega\mathbf{B}h. \tag{18}$$

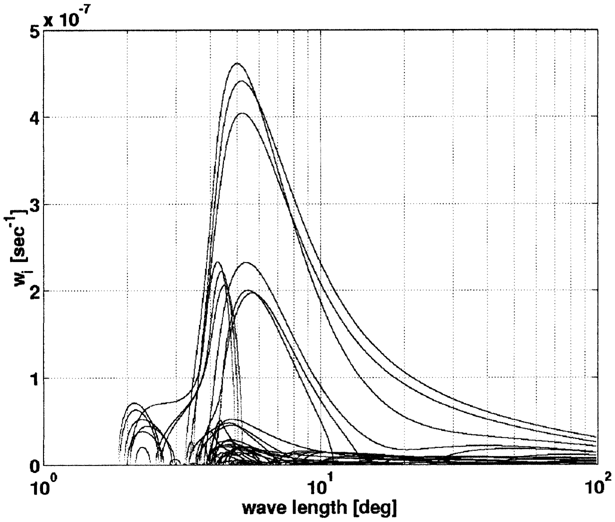

FIG. 10. The imaginary part of the eigenfrequency, ω_i, from the solutions of the eigenproblem as function of k for all horizontal locations in the region 10°–20°N, 170°–180°W.

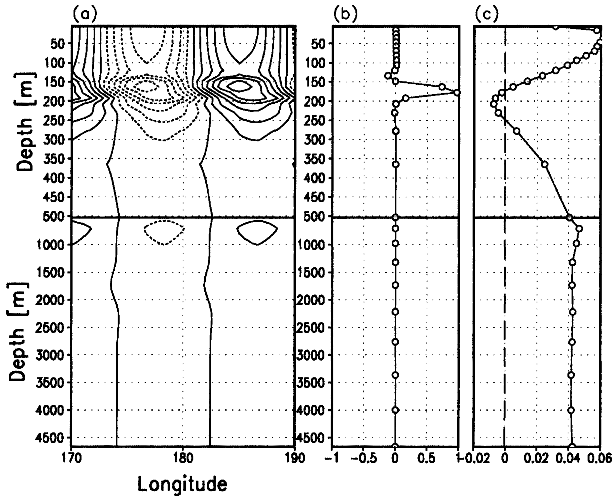

FIG. 11. (a) Reconstructed (in zonal) unstable solution of 15°N, 180° with zonal wave length of 15°. (b) The wave–mean flow energy transfer $\overline{v'T'}\partial\overline{u}/\partial z$ corresponding to the unstable waves. Note the large energy conversion at the critical layer at roughly 150-m depth. (c) $\overline{u} + (l/k)\overline{v} - \omega_r/k$ as function of depth. Note that the vertical axis scale is different between 1–500 and 500–4500 m.

We solved (18) at each horizontal model grid point with various choices for k and for $l = 2\pi/50°$ (reflecting the roughly westward average direction of propagation of the adjoint sensitivities). The imaginary part of the eigenfrequency from the solution of the eigenproblem as function of k and for all horizontal locations in the region 10°–20°N, 170°–180°W is shown in Fig. 10. There is a maximum growth at a wavelength around 5°. As will be shown below in an example, the solutions of (18) are not simply structured normal modes but have a more complicated structure due to the background shear, especially as a result of the existence of critical layers. The fastest westward propagating modes are now not necessarily those of a less complex vertical structure [as opposed to the classical normal modes theory, e.g., Killworth et al. (1997)]. In any case, our interest here is in finding the eigen solutions that are unstable and growing (like the adjoint sensitivities) and that have a similar vertical structure to that of the adjoint sensitivities.

Consider now eigensolutions whose eigenvalue is complex (unstable modes). If a complex eigenvalue exists, there also exist a complex eigenvector so that (15) may be written as

$$\psi' = [h_{\mathrm{Re}}(z) + ih_{\mathrm{Im}}(z)]e^{\omega_i t}e^{i(kx+ly-\omega_r t)}. \tag{19}$$

Rearranging (19) to separate the real part we find

$$\psi_r' = [h_{\mathrm{Re}}(z)^2 + h_{\mathrm{Im}}(z)^2]^{1/2}e^{\omega_i t} \times \cos[kx + ly - \omega_r t + \phi(z)], \tag{20}$$

where

$$\phi(z) = \tan^{-1}\frac{h_{\mathrm{Im}}(z)}{h_{\mathrm{Re}}(z)}. \tag{21}$$

We can now plot the unstable solution (20), (21) from some specific (x, y), reconstructed over a range of longitude (x) values, as seen in Fig. 11a, based on the unstable solution at 15°N, 180° and on a zonal wavelength of 15° chosen to match that of the adjoint sensitivities. Figure 11b shows the wave–mean flow energy transfer by the unstable waves, that is, the term $\overline{v'T'}\partial\overline{u}/\partial z = \overline{\psi_z'\psi_x'}\partial\overline{u}/\partial z$ (Pedlosky 1987), while Fig. 11c displays the term $\overline{u} + \overline{v}l/k - \omega_r/k$ from (17), showing where critical layers occur ($\overline{u}k + \overline{v}l - \omega_r = 0$. Note that the vertical shear at the latitude bands, in which we are mostly interested, is dominated by $\overline{u}$ so that the critical layers basically occur when $\overline{u} - \omega_r/k$ vanishes). The eigenvalue of the unstable solution, divided by k, is composed of the real $c_r = \omega_r/k = 0.04$ m s^{-1} and imaginary $c_i = \omega_i/k = 0.0016$ m s^{-1}, so the requirement that the imaginary part is much smaller than the real part is satisfied and the critical layer analysis can be applied (Pedlosky 1987).

There are a few things to note in Fig. 11. First, at the depth range where $\partial\overline{u}/\partial z$ is negative (200–500 m) the eigensolution is tilted in many horizontal locations to the east, according to the necessary condition for baroclinic instability (Pedlosky 1987, section 7.3). Second, at a depth of 150 m, where there exist a critical layer, there also exists a large energy transfer from the mean flow to the waves (Fig. 11b), as expected for baroclinic instability near a critical layer (Pedlosky 1987, section 7.8). Moreover, the solution is tilted strongly to the west. This is expected to happen in the vicinity of a critical layer if $\partial\overline{u}/\partial z$ is positive, as indeed occurs at the depth of 150 m, near the critical layer in Fig. 11c. The values of ω_i (Fig. 10) indicate that the e-folding growth time for perturbations is of the order of 1 yr. However, it turns out that the most unstable modes are actually sur-

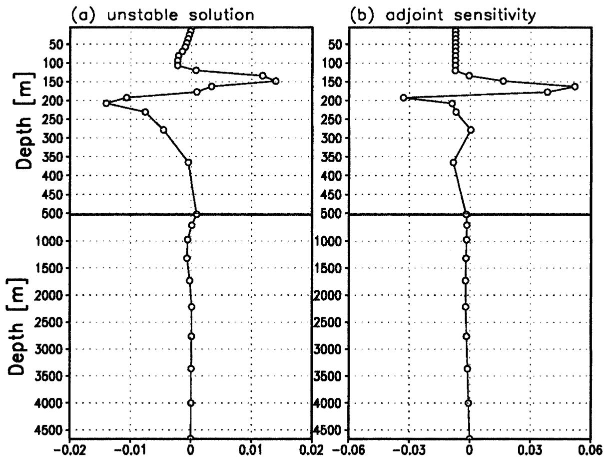

FIG. 12. (a) Vertical structure of temperature anomalies based on the normal mode solution of (18), $T' \sim \partial\psi'/\partial z$, of an unstable solution at 15°N, 180°. (b) The adjoint-calculated sensitivity to temperature perturbations at 15°N, 7 yr before time of cost function evaluation.

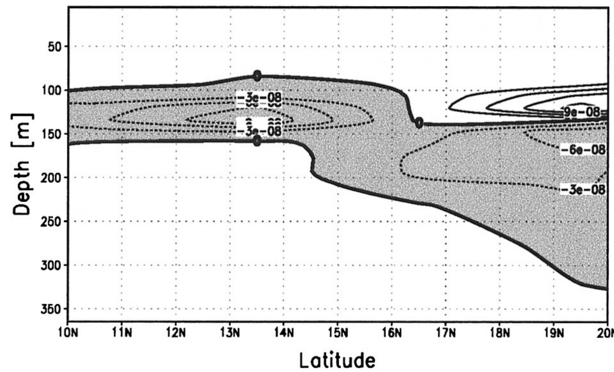

FIG. 13. A meridional cross section of the background meridional PV gradient $\partial\Pi/\partial y$ at 180° between 10° and 20°N. Negative values are shaded with gray and contour interval is 3×10^{-8}.

face trapped, while the normal modes that have larger amplitude at the depth range of 100–300 m, where the sensitivities have a maximum amplitude, have a growth time an order of magnitude longer, and a less obvious peak as function of k than seen in the modes that dominate Fig. 10.

The sensitivities we see in the adjoint model run (Fig. 2) have a wavelength of about 10°–15°. This wave length does not change when we double the various characteristic lengths defining the longitudinal, meridional, vertical, and temporal extent of the cost function (1). It therefore seems that the wavelength of the sensitivities is a property of the medium in which the sensitivities propagate. However, even when eliminating the surface trapped unstable modes, there is no clear maximum at 15° but rather a weak peak at 5° (amounting to plotting a subset of Fig. 10, not shown). This discrepancy might be a result of the model horizontal resolution, which is of 3°. Such a resolution does not properly resolve wavelengths of less than about 15° (five grid points per wavelength), therefore perhaps making the 15° wavelength the most unstable wave in the adjoint solution.

The adjoint sensitivities to temperature perturbations, $(\partial J/\partial T)_S$, are governed by the same dynamics of actual temperature perturbations. Now, the QG streamfunction calculated in the eigenproblem (18) is related to the temperature roughly as $\psi'_z \sim \rho' \sim \alpha T'$. In order to compare the vertical structure of the unstable mode with the adjoint sensitivity, we therefore need to plot both

$$\left(\frac{\partial J}{\partial T}\right)_S; \qquad \frac{1}{\alpha}\frac{\partial \psi'}{\partial z}. \tag{22}$$

Figure 12 shows the unstable solution of Fig. 11a, at 180°, along with a snapshot of the adjoint temperature sensitivity at the same location, seven years prior to the time of the cost function evaluation. The similarity of the two, in particular around the depth of the critical layer makes a very strong case that our adjoint sensitivities are indeed strongly affected by the presence of the critical layer. We note, however, that the normal modes and the adjoint sensitivity do not resemble each other at all times and locations as they do in this figure. The robust result, however, is that both have maximum amplitude at the same depth range and some abrupt vertical gradient near the depth of the critical layer at each horizontal location.

As another test of our hypothesis that the adjoint sensitivities, and therefore the midlatitude to Tropics waves teleconnection mechanism, are strongly influenced by baroclinic instability we examine whether the necessary conditions for instability are fulfilled. First, Fig. 11b shows that the vertically integrated energy transfer from the mean flow to the wave is positive, therefore the wave can be baroclinically unstable. Second, we plot the meridional gradient of the background PV ($\partial\Pi/\partial y$) at 180° (Fig. 13). It can be seen that the necessary condition for instability, requiring that $\partial\Pi/\partial y$ change sign, and therefore vanish on a line in the meridional section (Pedlosky 1987, p. 440), is fulfilled. Third, Fig. 14 shows the maximum imaginary eigenvalue ω_i for a wavelength of 15° as function of location of solution. Again there is a correspondence between the location of unstable regions calculated by the normal mode analysis and between the location of the strongest sensitivities calculated by the adjoint model.

In addition to the instability regions relevant to our sensitivity adjoint model results at the equatorward part of the subtropical gyres around 15°N and 12°S, our analysis also reveals instability regions at the poleward edges of the subtropical gyres. The reason these regions do not appear as clearly in the adjoint sensitivities is perhaps that the Rossby waves amplified there need to travel a longer distance toward the equator and manage to be damped before getting there.

We conclude this section by noting that all the analyses performed here strongly support the role of baro-

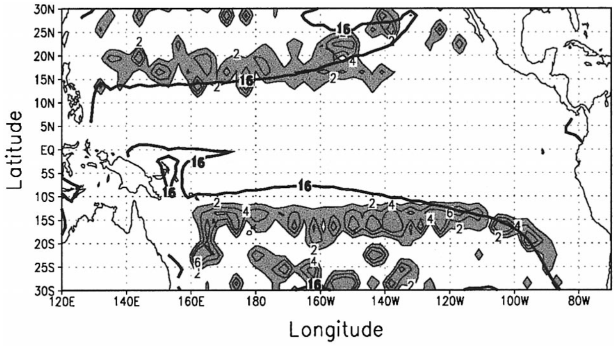

FIG. 14. Maximum imaginary frequency (ω_i s^{-1}) for a 15° wavelength. Only the unstable normal modes with a maximum amplitude below 100 m are plotted here, eliminating the surface trapped modes that are not relevant to the adjoint sensitivity solution (see text). Values larger than 5×10^{-8} s^{-1} are shaded with dark gray, and contour interval is 5×10^{-8} s^{-1}. The thick black line denotes the 16°C isotherm of the forward model climatology.

clinic instability in shaping the structure and path of propagation of the sensitivities as hypothesized in section 3c.

5. Conclusions

We proposed a specific novel mechanism for an ocean wave teleconnection between the midlatitude Pacific and the equator. According to this mechanism, baroclinically unstable areas of the subtropical gyre amplify waves passing via these areas. As a result, these amplified waves dominate the midlatitude signal at the equator. To do this analysis we have used the adjoint method of sensitivity analysis, as well as a quasigeostrophic normal-mode stability analysis. The comparison between the results of these two tools was especially useful in demonstrating the role of baroclinic instability in amplifying the sensitivity signal arriving at the equator from the midlatitudes. We demonstrated that critical layers due to the vertical shear of the subtropical gyre circulation in the baroclinically unstable areas play an important role in shaping the instability characteristics and the structure of the sensitivity signal seen in the adjoint model results.

Upon arrival to the equator, the midlatitude planetary waves can alter the stratification along the equator and thus produce a low-frequency modulation of the equatorial Pacific upper-ocean heat content due to the decadal-scale signal these waves carried from the midlatitudes. We did not address the question of what generates the midlatitude decadal signal, and many possibilities have been proposed in the literature (e.g., Gu and Philander 1997; Latif and Barnett 1994). An interesting observation possibly relevant to the present study is the maxima of Rossby wave signal seen at 10°S and 13°N, which are explained by Capotondi and Alexander (2003) in terms of the zonal coherence of Ekman pumping along these latitudes. One wonders if these bands of Rossby wave variability also indicate the importance of baroclinic instability at these locations, as found in the present study.

Our sensitivity analysis tool could, in principle, indicate also that the equatorial Pacific is sensitive to advection of midlatitude water, but showed a preferred ocean wave teleconnection. We verified that the sensitivity signal in our model is indeed due to waves by calculating dynamic (due to wave motion that moves the isopycnals) versus kinematic (due to long-isopycnal advection) sensitivities (Marotzke et al. 1999). We also conducted an idealized model run to demonstrate that, in the absence of baroclinically unstable regions, it is difficult for midlatitude waves to efficiently affect the equatorial Pacific.

It is obviously possible that some specific characteristics of our results are affected by the particular model used here. For example, the location and extent of the baroclinically unstable midlatitude regions could be different had we used a different viscosity. Similarly, advection might have been more dominant in a higher resolution model. Moreover, we cannot conclude whether the ocean wave teleconnection we presented here is dominant over other teleconnection mechanisms that include atmospheric bridges and coupled ocean–atmosphere feedback. However, we feel that the basic message here, of a wave teleconnection involving amplification by baroclinic instability, should hopefully be a robust result.

Acknowledgments. The detailed and most constructive comments of Antonietta Capotondi, Eyal Heifetz, and an anonymous reviewer are greatly appreciated. We thank Joe Pedlosky for his wonderful GFD book that was great help in this work. This study was partially funded by the Office of Global Programs (NOAA) and by the Israeli Science Foundation.

REFERENCES

An, S. I., and B. Wang, 2000: Interdecadal change of the structure of the ENSO mode and its impact on the ENSO frequency. *J. Climate*, **13,** 2044–2055.

Barnett, T., D. Pierce, M. Latif, D. Dommenget, and R. Saravanan, 1999: Interdecadal interactions between the tropics and midlatitudes in the pacific basin. *Geophys. Res. Lett.*, **26** (5), 615–618.

Capotondi, A., and M. A. Alexander, 2001: Rossby waves in the tropical north pacific and their role in decadal thermocline variability. *J. Phys. Oceanogr.*, **31,** 3496–3515.

——, and ——, 2003: Why are there Rossby wave maxima in the Pacific at 10°S and 13°N? *J. Phys. Oceanogr.*, **33,** 1549–1563.

Esbensen, S. K., and V. Kushnir, 1981: The heat budget of the global ocean: An atlas based on estimates from surface marine observations. Climate Research Institute Tech. Rep. 29, 27 pp.

Galanti, E., E. Tziperman, M. Harrison, A. Rosati, R. Giering, and Z. Sirkes, 2002: The equatorial thermocline outcropping—A seasonal control on the tropical Pacific ocean–atmosphere instability strength. *J. Climate,* **15,** 2721–2739.

——, ——, ——, ——, and Z. Sirkes, 2003: A study of ENSO prediction using a hybrid coupled model and the adjoint method for data assimilation. *Mon. Wea. Rev.*, in press.

Giering, R., cited 1999: Tangent linear and adjoint model compiler.

Users manual. [Available online at http://www.autodiff.com/tamc.]
——, and T. Kaminski, 1998: Recipes for adjoint code construction. *ACM Trans. Math. Soft.,* **24** (4), 437–474.
Gu, D., and S. G. H. Philander, 1997: Interdecadal climate fluctuations that depend on exchanges between the tropics and extratropics. *Science,* **275** (7), 805–807.
Hall, M. C. B., and D. G. Cacuci, 1983: Physical interpretation of the adjoint functions for sensitivity analysis of atmospheric models. *J. Atmos. Sci.,* **40,** 2537–2546.
Harper, S., 2000: Thermocline ventilation and pathways of tropical–subtropical water mass exchange. *Tellus,* **52A,** 330–345.
Hazeleger, W., M. Visbeck, M. Cane, A. Karspeck, and N. Naik, 2001: Decadal upper ocean temperature variability in the tropical Pacific. *J. Geophys. Res.,* **106** (C5), 8971–8988.
Jin, F. F., 2001: Low-frequency modes of tropical ocean dynamics. *J. Climate,* **14,** 3874–3881.
——, M. Kimoto, and X. C. Wang, 2001: A model of decadal ocean–atmosphere interaction in the North Pacific basin. *Geophys. Res. Lett.,* **28** (8), 1531–1534.
Killworth, P., D. Chelton, and R. D. Szoeke, 1997: The speed of observed and theoretical long extratropical planetary waves. *J. Phys. Oceanogr.,* **27,** 1946–1966.
Kleeman, R., J. P. Mccreary, and B. A. Klinger, 1999: A mechanism for generating ENSO decadal variability. *Geophys. Res. Lett.,* **26** (12), 1743–1746.
Latif, M., and T. P. Barnett, 1994: Causes of decadal climate variability over the North Pacific and North America. *Science,* **266,** 634–637.
Levitus, S. E., 1982: *Climatological Atlas of the World Ocean.* NOAA Prof. Paper 13, 173 pp. and 17 microfiche.
Liu, Z. Y., 1999a: Forced planetary wave response in a thermocline gyre. *J. Phys. Oceanogr.,* **29,** 1036–1055.
——, 1999b: Planetary wave modes in the thermocline: Non-Doppler-shift mode, advective mode and green mode. *Quart. J. Roy. Meteor. Soc.,* **125,** 1315–1339.
Lysne, J., P. Chang, and B. Giese, 1997: Impact of the extratropical Pacific on equatorial variability. *Geophys. Res. Lett.,* **24** (21), 2589–2592.
Marotzke, J., R. Giering, K. Q. Zhang, D. Stammer, C. Hill, and T. Lee, 1999: Construction of the adjoint MIT ocean general circulation model and application to Atlantic heat transport sensitivity. *J. Geophys. Res.,* **104** (C12), 29 529–29 547.
McPhaden, M. J., and D. Zhang, 2002: Slowdown of the meridional overturning circulation in the upper Pacific Ocean. *Nature,* **415,** 603–608.
Munk, W. H., 1981: Internal waves and small scale processes. *Evolution of Physical Oceanography,* B. A. Warren and C. Wunsch, Eds., The MIT Press, 264–291.
Pacanowski, R. C., and S. G. H. Philander, 1981: Parameterization of vertical mixing in numerical models of tropical oceans. *J. Phys. Oceanogr.,* **11,** 1443–1451.
——, and S. M. Griffies, 1999: *MOM 3.0 Manual,* 671 pp. [Available from NOAA/Geophysical Fluid Dynamics Laboratory, Princeton, NJ, 08542.]
Pedlosky, J., 1987: *Geophysical Fluid Dynamics.* 2d ed. Springer-Verlag, 710 pp.
Reynolds, R. W., and T. M. Smith, 1994: Improved global sea surface temperature analyses using optimum interpolation. *J. Climate,* **7,** 929–948.
Roemmich, D., and J. Gilson, 2001: Eddy transport of heat and thermocline waters in the North Pacific: A key to interannual/decadal climate variability? *J. Phys. Oceanogr.,* **31,** 675–687.
Schneider, N., S. Venzke, A. J. Miller, D. W. Pierce, T. P. Barnett, C. Deser, and M. Latif, 1999: Pacific thermocline bridge revisited. *Geophys. Res. Lett.,* **26** (9), 1329–1332.
Stricherz, J. N., J. J. O'Brien, and D. M. Legler, 1992: *Atlas of Florida State University Tropical Pacific Winds for TOGA 1966–1985.* Florida State University, 250 pp.
——, D. Legler, and J. J. O'Brien, 1997: *Indian Ocean.* Vol. III, TOGA *Pseudo-Stress Atlas 1985–1994.* Florida State University, 155 pp.
Syu, H. H., and J. D. Neelin, 2000: ENSO in a hybrid coupled model. Part I: Sensitivity to physical parameterizations. *Climate Dyn.,* **16,** 19–34.
Trenberth, K. E., and J. W. Hurrell, 1994: Decadal atmosphere–ocean variations in the Pacific. *Climate Dyn.,* **9** (6), 303–319.
Zhang, R. H., T. Kagimoto, and S. E. Zebiak, 2001: Subduction of decadal North Pacific thermal anomalies in an ocean GCM. *Geophys. Res. Lett.,* **28** (12), 2449–2452.